Contribution from the Department of Chemistry and Biochemistry, University of Windsor, Windsor, Ontario N9B 3P4, Canada

EPR Study of Manganese(II) in Two Crystalline Forms of $Fe(C_6H_8N_2S_2)_2(NCS)_2$ and the High-Spin-Low-Spin Transition That Occurs in Only One Form. X-ray Structure Determination of Both Forms

Andrzej Ozarowski, Bruce R. McGarvey,* Anil B. Sarkar, and John E. Drake

Received June 3, 1987

Two crystalline forms of bis(2,2'-bi-2-thiazoline)bis(thiocyanato)iron(II), $Fe(C_6H_8N_2S_2)_2(NCS)_2$, were obtained. While one of them (polymorph A) shows the high-spin-low-spin transitions with a hysteresis over the temperature range ca. 170-180 K, in agreement with the literature data, the other one (polymorph B) is paramagnetic over the temperature range 77-300 K. The X-ray data are (data in parentheses refer to the polymorph B): crystal system triclinic (triclinic), space group $P\bar{1}$ ($P\bar{1}$), a = 8.521 (8) Å (10.846 (3) Å), b = 11.063 (9) Å (10.847 (3) Å), c = 12.498 (6) Å (12.526 (4) Å), α = 96.83 (4)° (115.72 (2)°), β = 91.81 (6)° (93.92 (2)°), γ = 106.24 (6)° (119.97 (2)°), V = 1120 (1) Å^3 (1070 (1) Å^3), Z = 2 (2), and R = 0.0481 (0.0490). The molecules building up both crystal lattices have the cis configuration and are very similar. The single crystals of both kinds, doped with Mn(II), were investigated by electron paramagnetic resonance spectroscopy. The magnitudes of the zero-field-splitting parameters for the Mn(II) ion and the orientation of the ZFS tensor found both above and below the "crossover" temperature suggest that the spin transition does not cause major changes of the molecular symmetry. A considerable slowing down of the spin transition rate in the large single crystals with respect to the powder samples was detected by EPR. The line widths observed for the low-spin resonance observed during the spin transition in the single crystal are inconsistent with the domain sizes proposed for this transition by earlier studies on powders.

Introduction

Spin-state transitions are encountered in (approximately) octahedral complexes of the first-row transition metals with configurations d^4 to d^7 if the crystal field splitting, $10Dq$, is comparable with the spin-pairing energy. In the case of iron(II) ion in octahedral symmetry the "crossover" of the $^1A_1((t_2)^6)$ and $^5T_2((t_2)^4(e)^2)$ high spin state occurs if

$$10Dq = 2.195B + 3.708C$$

where B and C are the Racah parameters of interelectronic repulsion.[1,2] Deviations from ideal octahedral symmetry do not affect essentially the spin transitions.

The "crossover" phenomena can be generally classified into two types: (1) discontinuous, i.e., transitions occurring over a narrow temperature range and showing hysteresis, and (2) gradual, occurring over an extended temperature range without hysteresis. Various physical methods have been applied to study the crossover in iron(II) compounds.[1-11] The results suggest in general a cooperative nature for the phenomenon.

A very abrupt spin-state transition was discovered in the title compound by Bradley et al.[3] The same authors suggested a cis configuration for the complex on the basis of the IR spectra. Further studies, using Mössbauer spectroscopy,[4] powder X-ray diffraction,[4] magnetic susceptibility measurements,[5] and calorimetry,[6] revealed the first-order character of the phase transition. A pronounced thermal hysteresis was observed: the transition took place at 171.2 K by cooling and at 180.9 K by warming up, suggesting the formation of noninteracting domains containing either high-spin or low-spin molecules. (The temperatures varied somewhat depending on the preparation and sample treatment.[5]) The average number of molecules constituting a single domain was estimated as 50-55.[6] It seemed to us that the EPR technique of looking at the molecules rather than at the bulk properties of the crystal lattice could give some new information about the spin-state transitions. Since low-spin iron(II) is diamagnetic and the high-spin ion is usually EPR silent owing to the very large zero-field splitting (ZFS) and/or the very short relaxation time, both typical for the even-electron systems, we had to introduce the manganese(II) impurities in order to probe the behavior of the iron ions. A similar technique has been employed before to monitor the ferroelectric phase transitions in many materials.[12] An EPR study on the "crossover" phenomena in powders of other Fe(II) compounds has been reported upon by this laboratory.[7] During our attempts to grow single crystals of the title complex, we discovered that two kinds of crystals formed depending on the recrystallization conditions. Only one of them, which will be called polymorph A throughout the text, exhibited the "crossover" behavior. Large single crystals of both substances, doped with Mn(II), were prepared and investigated by EPR. X-ray-quality crystals (without Mn) were prepared, also, and the structures were determined.

Experimental Section

A. Preparation of Compounds. 1. 2,2'-Bi-2-thiazoline (BT). Dithiooxamide (rubeanic acid) was reacted with 2-aminoethanol (molar ratio 1:2) in ethanolic solution at room temperature to form *N*,*N*'-bis(2-hydroxyethyl)dithiooxamide, which was filtered, recrystallized from ethanol, and reacted with thionyl chloride in toluene, forming 2,2'-bi-2-thiazoline dihydrochloride. This was filtered off and neutralized with an aqueous solution of sodium bicarbonate, yielding 2,2'-bi-2-thiazoline, which was purified by Soxhlet extraction with hexane, followed by recrystallization from ethanol. A white crystalline product was obtained.[13]

2. $Fe(BT)_2(NCS)_2$. Iron(II) thiocyanate solution was obtained in the reaction of ethanolic solutions of iron(II) chloride dihydrate and potassium thiocyanate. The resulting KCl was filtered off, and the hot solution was added dropwise with stirring to the hot ethanolic solution of the ligand. The quickly formed compound was filtered off and purified by Soxhlet extraction with ethanol. Quite large black shining crystals could be obtained. The analogous manganese complex was prepared in a similar way and recrystallized from methanol (without Soxhlet extraction).

B. Growth of Single Crystals. 1. Polymorph A. A 1.0-g sample of $Fe(BT)_2(NCS)_2$ was dissolved in 200 mL of hot ethanol. The solution was filtered and poured into a three-necked flask placed in an oil bath with a temperature of 78 °C. A weak jet of nitrogen was blown through the flask (above the solution) for 1 week, causing evaporation of two-thirds of the solvent. A large number of crystals of various sizes were obtained. Crystals had the shape of elongated parallelepipeds. The same form was obtained also from hot methanolic solutions of the complex.

* Author to whom correspondence should be addressed.

(1) Gütlich, P. *Struct. Bonding (Berlin)* **1981**, *44*, 83.
(2) König, E.; Ritter, G.; Kulshreshtha, S. K. *Chem. Rev.* **1985**, *85*, 219.
(3) Bradley, G.; McKee, V.; Nelson, S. M. *J. Chem. Soc., Dalton Trans.* **1978**, 522.
(4) König, E.; Ritter, G.; Irler, W.; Nelson, S. M. *Inorg. Chim. Acta* **1979**, *37*, 169.
(5) Müller, E. W.; Spiering, H.; Gütlich, P. *J. Chem. Phys.* **1983**, *79*, 1439.
(6) Kulshreshtha, S. K.; Sasikala, R.; König, E. *Chem. Phys. Lett.* **1986**, *123*(3), 215.
(7) Rao, P. S.; Reuveni, A.; McGarvey, B. R.; Ganguli, P.; Gütlich, P. *Inorg. Chem.* **1981**, *20*, 204.
(8) Rao, P. S.; Ganguli, P.; McGarvey, B. R. *Inorg. Chem.* **1981**, *20*, 3682.
(9) Hauser, A.; Gütlich, P.; Spiering, H. *Inorg. Chem.* **1986**, *25*, 4245.
(10) Franke, P. L.; Haasnoot, J. G.; Zuur, A. P. *Inorg. Chim. Acta* **1982**, *59*, 5.
(11) Herber, R. H. *Inorg. Chem.* **1987**, *26*, 173.
(12) Navalgund, R.; Gupta, L. C. *Solid State Commun.* **1976**, *19*, 1205.
(13) Nelson, J.; Nelson, S. M.; Perry, W. D. *J. Chem. Soc., Dalton Trans.* **1976**, 1282.

0020-1669/88/1327-0628$01.50/0 © 1988 American Chemical Society

Table I. Summary of Crystal Data and Data Collection Parameters

	polymorph A	polymorph B
formula	$C_{14}H_{16}N_6S_6Fe$	$C_{14}H_{16}N_6S_6Fe$
mol wt	516.56	516.56
cryst syst	triclinic	triclinic
space group	$P\bar{1}$	$P\bar{1}$
a, Å	8.521 (8)	10.846 (3)
b, Å	11.063 (9)	10.847 (3)
c, Å	12.498 (6)	12.526 (4)
α, deg	96.83 (5)	115.72 (2)
β, deg	91.81 (6)	93.92 (2)
γ, deg	106.24 (6)	119.97 (2)
V, Å^3	1120 (1)	1070 (1)
Z	2	2
d(calcd), g cm^{-3}	1.53	1.63
d(measd), g cm^{-3}	1.52	1.62
cryst size, mm	0.31 × 0.19 × 0.12	0.46 × 0.46 × 0.19
μ(Mo Kα), cm^{-1}	11.66	12.44
diffractometer	Syntex $P2_1$	Syntex $P2_1$
radiation, λ, Å	0.709 26	0.709 26
temp, °C	20	20
scan method	θ–2θ	θ–2θ
data collection range, deg	4–44 (h,±k,±l)	4–45 (h,±k,±l)
scan speed, deg min^{-1}	2.02–4.88	2.02–4.88
no. of total reflns measd	2332	2824
no. of unique data used	1544 [$I > 3\sigma(I)$]	1749 [$I > 3\sigma(I)$]
no. of params	174	174
residual factors R, R_w	0.0481, 0.0515	0.0490, 0.0521
largest shift/esd (final)	0.002	0.002
largest $\Delta\rho$ in diff Fourier, e Å^{-3}	0.39	0.49

The analysis was performed by Galbraith Laboratories Inc., Knoxville, TN. Anal. Found: C, 32.28; H, 3.01; N, 16.11; S, 37.21; Fe, 10.41. Calcd for $FeC_{14}H_{16}N_6S_6$: C, 32.55; H, 3.12; N, 16.27; S, 37.24; Fe, 10.81.

2. Polymorph B. A 0.5-g sample of $Fe(BT)_2(SCN)_2$ was dissolved in 100 mL of methanol or in 200 mL of ethanol at room temperature. The filtered solution was poured into a three-necked flask, and a weak nitrogen stream was blown for a few weeks. Crystals of a shape different from that of polymorph A were formed (octahedra with cut-off corners). The analysis was performed by Galbraith Laboratories Inc., Knoxville, TN. Anal. Found: C, 31.54; H, 2.94; N, 16.20; S, 37.09; Fe, 10.89. Calcd for $FeC_{14}H_{16}N_6S_6$: C, 32.55; H, 3.12; N, 16.27; S, 37.24; Fe, 10.81.

3. Mn(II)-Doped Crystals. The Mn(II)-doped crystals were obtained in similar ways, by adding to the mother liquors 5% of $Mn(BT)_2(SCN)_2$ with respect to the amount of $Fe(BT)_2(SCN)_2$. (Since the manganese compound is much more soluble than the iron compound, the crystals contain less than 5% of Mn with respect to Fe.) The dimensions of the largest doped crystals of both kinds were ca. 5 × 3 × 2 mm. Their single-crystal nature was confirmed by the EPR spectra.

C. EPR Spectra. EPR spectra were recorded on a Varian E12 spectrometer equipped with a rotating cavity and rotating base magnet. The single crystals were mounted on quartz rods. The Varian nitrogen-flow cooling system was used to perform the variable-temperature studies. The insert type Dewar was employed to record the spectra at the fixed temperature 77 K. The magnetic field and field sweeps were regulated by a Hall probe. Both the linearity and absolute field strengths were measured by using a home-built variable-frequency proton NMR spectrometer whose frequency was measured by a frequency counter.

D. Structure Determination and Refinement. Suitable crystals of the two crystalline modifications, A and B, were sealed in capillary tubes and mounted on a Syntex $P2_1$ four-circle diffractometer equipped with a scintillation counter and graphite monochromator. The unit cell dimensions, listed in Table I, were obtained from a least-squares refinement of the setting angles of 15 reflections in the $15 < 2\theta < 35°$ range. The space group $P\bar{1}$ was used for both forms and later assumed correct because of the successful refinement of both structures. The data were collected by using the θ–2θ scan technique in a manner described in detail elsewhere;[14] the details of other pertinent X-ray data are given in Table I. The stability of the crystals in the X-ray beam was monitored by three reflections, and no significant change in the intensities was noted. The data were corrected for Lorentz and polarization effects, and no absorption correction was required. For A, the position of the Fe atom was located from an E map generated by SHELX 77. Structure B was solved by MULTAN 78.[15] A series of subsequent difference Fourier maps revealed the positions of all the remaining non-hydrogen atoms. The amount of data did not allow us to refine the carbon atoms anisotropically in the final model. Least-squares refinement minimizing the function $\sum w(|F_o| - |F_c|)^2$ converged at $R = \sum(||F_o| - |F_c||)/\sum|F_o| = 0.0481$ (A) or 0.0490 (B) and $R_w = [\sum w(||F_o| - |F_c||)^2/\sum w|F_o|^2]^{1/2} = 0.0515$ (A) or 0.0521 (B). In the final stages hydrogen atoms were included in idealized positions (C–H = 0.95 Å, H–C–H = 109.5°) with isotropic U's set at 0.1 Å^2 greater than those of the corresponding carbon atoms. A weighting scheme of the form $w = 1/\sum[\sigma^2(F) + pF^2]$ was employed with a final p value of +0.000 606 for A. In the last cycle no parameters changed by more than 0.002σ (A or B). No evidence of secondary extinction was found. Sources of computer programs and scattering factors have been previously described.[14,16]

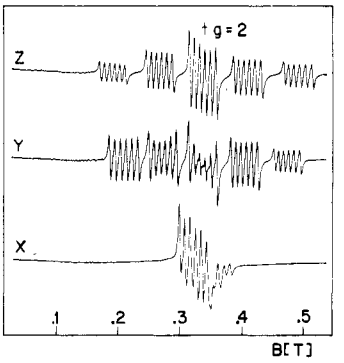

Figure 1. Single-crystal X-band EPR spectra (9.54 GHz, 293 K) of polymorph A of $Fe(BT)_2(NCS)_2$ measured at three principal orientations. $g = 2$ corresponds to 0.3404 T.

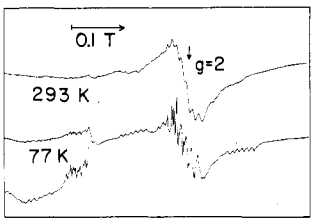

Figure 2. Powder EPR spectra of polymorph A recorded at 9.10 GHz. $g = 2$ corresponds to 0.3247 T.

Results

A. EPR Results. 1. Polymorph A. The single-crystal EPR spectra, as well as the spectra of powder samples obtained by grinding of the crystals, showed typical features for a $S = {}^5/_2$, $I = {}^5/_2$ system with the zero-field splitting comparable to the microwave quantum energy (at the X-band frequency). Five fine "allowed" components split further by the nuclear hyperfine interaction into six lines each were clearly visible at certain orientations of the crystals (see Figure 1). In the powder spectra the outermost fine components corresponding to $H \| Z$ were very weak. They could be detected at higher gain, however. As the temperature of the powder sample was lowered, the various features appeared to broaden and became less distinct. However, when the temperature of 170 K was reached (very near to the reported HS–LS transition temperature of 171.2 K), the spectrum abruptly changed to one with very sharp features, indicating a distinct change in the environment of the Mn ions. This sharp-line spectrum was then observed down to 77 K (Figure 2). The subsequent warming up of the sample resulted in the broad-line spectrum reappearing abruptly at ca. 180 K. Thus, we were able with EPR to detect the same hysteresis, within the error limits, as found by susceptibility measurements,[5] Mössbauer spectroscopy,[4] and calorimetry.[6] It is tempting to ascribe this apparent broadening to the presence of paramagnetic iron above the transition temperature. If the lifetime, τ_{1e}, of a spin state is very short in Fe(II), then the magnetic field generated by a para-

(14) Chadha, R. K.; Drake, J. E.; Sarkar, A. B. *Inorg. Chem.* **1986**, *25*, 2201.
(15) Germain, G.; Main, P.; Woolfson, M. M. *Acta Crystallogr., Sect. A: Cryst. Phys., Diffr., Theor. Gen. Crystallogr.* **1971**, *A27*, 368.
(16) Forsyth, J. B.; Wells, M. *Acta Crystallogr.* **1959**, *12*, 412.

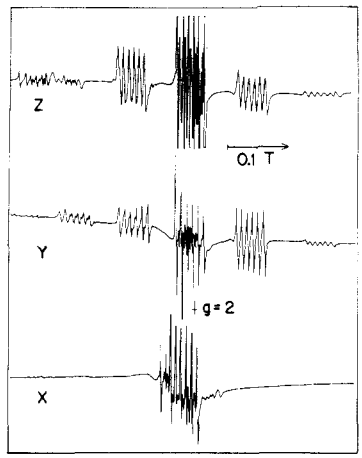

Figure 3. Single-crystal EPR spectra (9.07 GHz, 77 K) of polymorph A of $Fe(BT)_2(NCS)_2$ (diamagnetic phase) measured at three principal orientations. $g = 2$ corresponds to 0.3236 T. The peaks of the extremely intense signals in the central part of the top spectrum are cut off.

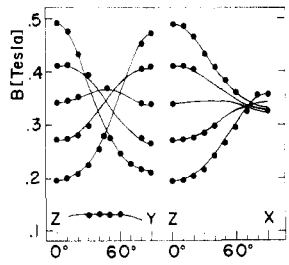

Figure 4. Angular dependencies of the transition fields for polymorph A of $Fe(BT)_2(NCS)_2$ (9.54 GHz, 293 K): (left) rotation around the X axis; (right) rotation around the Y axis. Solid lines are calculated with the parameters from Table II. The bottom part of the left plot shows the strongest "forbidden" transition. At some intermediate orientations only the positions of the outer fine components could be measured owing to the overlap.

magnetic Fe(II) in its vicinity is proportional to χR^{-3}, where χ is the atomic susceptibility and R is the distance. In this case magnetic fields seen by Mn(II) from neighboring Fe(II) ions would be less than 0.1 G and would produce no appreciable broadening. For very long τ_{1e}'s the magnetic fields would be on the order of 100 G. It may be that we are in the transitional region and are seeing the results of τ_{1e} becoming longer as the temperature is lowered. The broadening could also be due to strain effects causing a distribution of zero-field interactions in the Mn(II) complex throughout the crystal.

The single crystals that were cooled to temperatures below the HS–LS transition cracked and pulverized when attempts were made to warm them up above the LS–HS transition temperature. No crystal was found that could survive the LS–HS transition, while all crystals examined passed through the transition in the opposite sense without damage.

Since the spectrum of only one manganese was observed at any orientation (Figures 1 and 3), the orientation of the three principal axes was obtained by a direct method. First the crystal was rotated until the orientation having the maximum separation of fine structure components was found. This direction was taken to be the Z principal axis. The crystal was then rotated with the magnetic field perpendicular to this Z axis to locate the X and Y principal orientations. In this rotation the Y direction is defined as the direction having a maximum separation in the fine-structure components. Finally, the angular dependencies of the resonance fields were measured by rotating the crystals with the magnetic field perpendicular to the principal axes X, Y, and Z, respectively (Figure 4).

Single-crystal EPR spectra measured at three principal orientations are shown in Figures 1 and 3. The spectra are nicely resolved for both the paramagnetic phase at room temperature and for the diamagnetic phase below the "crossover" temperature.

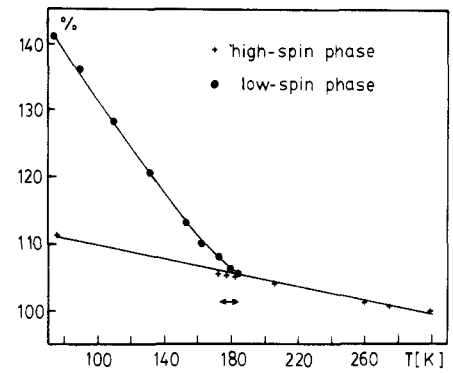

Figure 5. Temperature dependence of the total zero-field splitting measured for a single crystal of polymorph A at $H \| Z$. The magnitude of the splitting at 300 K is assumed as 100%. The arrow indicates the hysteresis loop range.

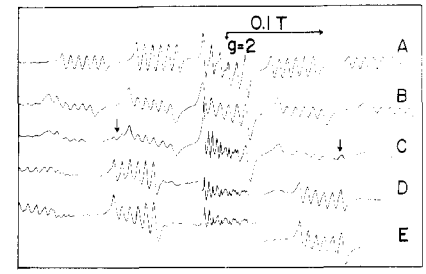

Figure 6. Single-crystal EPR spectra measured for polymorph A with the magnetic field nearly parallel to the Z axis: (A) at room temperature; (B) at 77 K, 5 min after cooling (pure paramagnetic phase); (C) at 77 K, 30 min after cooling (arrows indicate the signals due to the slowly forming low-spin phase); (D) at 77 K, 40 min after cooling; (E) at 77 K, 60 min after cooling (nearly pure low-spin phase). The central parts of spectra D and E were recorded with the gain reduced 100 times.

The forbidden transitions could be clearly observed in the 77 K spectrum, being considerably narrower than the allowed signals. The effect of the nuclear quadrupole splitting upon the spectrum could be observed at all temperatures. The magnitude of the zero-field splitting was very strongly temperature dependent in the diamagnetic phase, but less so in the paramagnetic phase (Figure 5). The spectra due to only one entity were observed at all orientations of the crystals, thus suggesting strongly that the unique symmetry element in the unit cell is the inversion center.

Whenever a single crystal was taken below the transition temperature, it was observed that the spectrum changed with time and was reproducible only after a period of time greater than $^1/_2$ h. The following experiment was, therefore, done to follow the time dependence of the phase transition: The crystals were oriented with $H \| Z$ or $H \| Y$ in the insert Dewar at room temperature, and then liquid nitrogen was poured into the Dewar and the time evolution of the spectra was followed. (The crystals were in direct contact with the liquid-nitrogen bath.) It was found that the transition took a very long time. During the first minutes following cooling, the spectrum due to the high-spin species was observed with slightly impaired resolution and with the ZFS parameters larger by some 11% with respect to the room-temperature magnitudes (Figure 6). Subsequently, the spectra of the low-spin phase could be observed, with a considerably larger zero-field splitting. These new signals were narrower, particularly in the central part of the spectra. The intensity of the high-spin spectrum decayed continuously while the intensity of the spectrum due to the low-spin phase increased at the same time. Approximately 1 h was required to achieve the complete transition. No signals due to any intermediate phase could be detected. A powder sample obtained by grinding the crystals did not exhibit any delay of the high-spin–low-spin phase transition. We were able to record the first EPR spectrum as soon as ca. 90 s after cooling, and only the spectrum of the low-spin species was seen and did not change any further with time. The transition from low- to high-spin state could be not followed for the single crystals for reasons stated earlier.

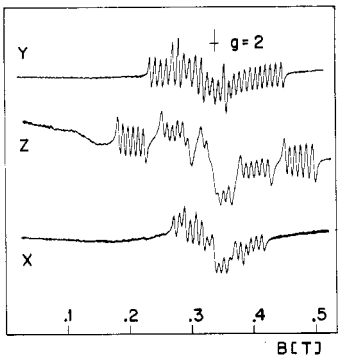

Figure 7. Single-crystal EPR spectra (9.51 GHz, 293 K) of polymorph B measured at three principal orientations. $g = 2$ corresponds to 0.3393 T.

2. Polymorph B. The room-temperature spectra measured at three principal orientations of the single crystals suggested at first sight similar D parameters but a very different E value from those for polymorph A (Figure 7). As the temperature was lowered, the zero-field splitting increased and the hyperfine features became less well resolved due to the increasing line width. The line widths increased continuously as the crystals (or powder samples) were cooled down to 77 K, where the hyperfine structure was hardly detectable. Thus, the host lattice is paramagnetic and no phase transition occurs in the temperature range examined (77–300 K). The cooling down to 77 K and subsequent warming up to room temperature did not cause any damage to these crystals. The spectrum of only one molecular entity was observed at all orientations.

3. Evaluation of Spin Hamiltonian Parameters. Since we were mainly interested in the fine-structure components of the spin Hamiltonian and any change in these parameters with temperature, a complete analysis of the spin Hamiltonian was not attempted.

At the orientation $H \| Z$ (maximal splitting) the distances between the central and the inner fine components were different from those between the inner and outer fine components (for both compounds). Hence, there was an obvious necessity to include the fourth-order terms in the spin Hamiltonian in addition to the second-order terms. The spin Hamiltonian used in this study was

$$\hat{H} = \beta B \cdot \mathbf{g} \cdot \hat{\mathbf{S}} + D[\hat{S}_z^2 - S(S+1)/3] + E(\hat{S}_x^2 - \hat{S}_y^2) + (\alpha/384)(112\hat{S}_z^4 - 760\hat{S}_z^2 + 567) + (\alpha/48)(\hat{S}_+^4 + \hat{S}_-^4) \quad (1)$$

Only the cubic part of the term containing the fourth-power spin operators was taken into account. The form of the Hamiltonian was taken from ref 17. It is equivalent to that given in ref 18–20, as far as the cubic part is concerned. The (complex, in general) matrix of the Hamiltonian was diagonalized by using the Householder transformation.[21] All possible transition fields and respective transition probabilities were found over the magnetic field range 0–0.6 T. All calculations were performed on a Commodore 64 computer using our own programs. The time required for the above calculation was ca. 50 min when a standard BASIC program was used or ca. 12 min when the compiled program was used. The parameters of the spin Hamiltonian were found by fitting of the spectra measured at the principal orientations, which are shown in Figures 1, 3, and 7. These orientations were very easy to find for polymorph A, which was fortunate, since we needed a new crystal for each low-temperature experiment. The magnetic field strengths at the centers of the hyperfine patterns were assumed to be the correct resonance fields for the fine components of the spectra (see below). The values of D, E, and α found for both substances are given in Table II. The g value is equal to 2, as expected for the $^6A_1(^6S)$ ground term of Mn(II). The calculated positions of the signals deviated from the experimental values by less than 20 G, except for the second "allowed" features at $H \| Z$ and $H \| Y$. The possible reasons for the errors are as follows: (1) The hyperfine and nuclear quadrupole interactions were not taken into account. (2) The noncubic fourth-order terms were neglected. (3) Some errors in the orientations of the crystals were unavoidable. In our opinion, the agreement between the calculated and experimental resonance fields was satisfactory. Finally, the ZFS parameters found in this way were used to calculate the angular dependencies of the spectra for each of the rotations about the principal axes, showing a reasonably good agreement with experiment (Figure 4). While the D parameters were rather similar for both crystalline forms, the E values differed considerably. The E/D ratio for polymorph B was near the limiting value of 0, thus suggesting a pseudoaxial symmetry for the molecule. Polymorph A with its E/D ratio near the limiting value of $^1/_3$ would appear to possess very little symmetry. A second-order perturbation calculation was performed to account for the hyperfine splitting, which was different for various fine components of the spectra of both crystal forms. For polymorph A with $H \| Z$, the hyperfine splitting was 82 G for the first fine "allowed" group and 92 G for the last one. An opposite trend (93 and 84 G, respectively) was observed for $H \| Y$. A similar behavior was found for polymorph B. The variation of the hyperfine splitting depends on the signs of the ZFS parameters versus the sign of the hyperfine constant.[18,22] The eigenfunctions of the Hamiltonian (1) multiplied by the eigenfunctions of the $\hat{I}_z$ operator were used as the basis set. The correct trends and magnitudes for the variation of the hyperfine splitting were calculated (for $H \| Z$ and $H \| Y$) by assuming opposite signs for the hyperfine constant and the D parameter. Since the hyperfine constant is always negative, the ZFS parameters D, E, and α for both crystal forms are positive. (The relative signs of D, E, and α were found to be the same by the fitting procedures described above.) The value of −88 G for the hyperfine constant was found. The simple perturbation calculation broke down at $H \| X$ and for the second fine components at $H \| Z$ and $H \| Y$ corresponding to 77 K. The hyperfine interactions also shifted the centers of the fine features (with respect to those calculated without the hyperfine structure). The calculated shifts were smaller than 20 G, however, and were disregarded.

Table II. Zero-Field-Splitting Parameters for the Mn(II) Ion (10^{-4} cm^{-1})

		D	E	α
polymorph A	293 K	342	91	8.0
	77 K, high-spin phase	380		
	77 K, low-spin phase	495	150	7.5
polymorph B	293 K	309	29	7.9
	77 K	~340		

4. NMR Spectra. Measurements of the temperature dependence of line widths for powder NMR spectra were performed over the temperature range 140–300 K by using a Bruker CPX-90 pulse NMR spectrometer. The line width of polymorph A increased linearly with $1/T$ from 66 kHz at 280 K to 81 kHz at 186 K and then abruptly fell to 54 kHz at 178 K and was subsequently temperature independent down to 140 K. Hence, the spin-crossover transition was detected at the expected temperature by this method.[8] The line width of polymorph B did not exhibit any discontinuous changes over the entire temperature range (140–300 K). At the lowest temperatures the signals due to the two types of protons became distinguishable. This can be explained only if the iron ion was paramagnetic at all temperatures studied. Hence, the conclusion of no spin transition in this crystalline form made on the basis of the EPR spectra is confirmed by NMR.

(17) Wertz, J. E.; Bolton, J. R. In *Electron Spin Resonance: Elementary Theory and Practical Applications*; McGraw-Hill: New York, 1972; p 303.
(18) Abragam, A.; Bleaney, B. In *Electron Paramagnetic Resonance of Transition Ions*; Clarendon: Oxford, England, 1970; p 436.
(19) Bencini, A.; Gatteschi, D. In *Transition Metal Chemistry*; Melson, G. A., Figgis, B. N., Eds.; Marcel Dekker: New York, 1982; Vol. 8, p 33.
(20) McGarvey, B. R. In *Transition Metal Chemistry*; Carlin, R. L., Ed.; Marcel Dekker: New York, 1966; Vol. 3, p 169.
(21) Wilkinson, J. H. In *The Algebraic Eigenvalue Problem*; Clarendon: Oxford, England, 1965; p 290.
(22) Goodgame, M.; Okey, J. N. *J. Chem. Soc., Dalton Trans.* **1985**, 75.

Table III. Atomic Coordinates and Isotopic Thermal Parameters (10^3 Å^2) for Polymorph A of $Fe(C_6H_8N_2S_2)_2(NCS)_2$[a]

atom	x	y	z	U_{eq}[b]
Fe	−0.0518 (1)	0.2096 (1)	0.2594 (1)	45 (1)
S(1)	−0.3859 (3)	−0.1945 (2)	0.1313 (2)	82 (2)
S(2)	−0.2839 (3)	−0.0175 (3)	−0.0699 (2)	83 (2)
S(3)	−0.4404 (3)	0.4238 (3)	0.3448 (2)	86 (2)
S(4)	−0.2391 (4)	0.3844 (3)	0.5669 (2)	94 (2)
S(5)	0.2594 (3)	0.5739 (3)	0.1105 (2)	92 (2)
S(6)	0.3792 (3)	0.0453 (3)	0.3829 (2)	93 (2)
N(1)	−0.2225 (7)	0.0180 (6)	0.2474 (5)	50 (4)
N(2)	−0.1018 (7)	0.1408 (6)	0.0862 (4)	46 (4)
N(3)	−0.2648 (7)	0.2903 (6)	0.2507 (5)	48 (4)
N(4)	−0.0981 (8)	0.2668 (6)	0.4250 (5)	52 (4)
N(5)	0.0947 (8)	0.3802 (6)	0.2190 (5)	57 (5)
N(6)	0.1345 (8)	0.1408 (7)	0.3111 (5)	64 (5)
C(1)	−0.2703 (9)	−0.0379 (7)	0.1515 (6)	50 (2)
C(2)	−0.3993 (12)	−0.1913 (9)	0.2759 (7)	87 (3)
C(3)	−0.2702 (10)	−0.0709 (8)	0.3272 (7)	65 (3)
C(4)	−0.2133 (9)	0.0348 (7)	0.0628 (6)	45 (2)
C(5)	−0.1396 (10)	0.1178 (8)	−0.1109 (7)	66 (3)
C(6)	−0.0523 (10)	0.2021 (7)	−0.0093 (6)	53 (2)
C(7)	−0.2973 (9)	0.3378 (7)	0.3414 (6)	50 (2)
C(8)	−0.4911 (12)	0.3696 (9)	0.2036 (7)	84 (3)
C(9)	−0.3511 (10)	0.3217 (9)	0.1606 (7)	68 (3)
C(10)	−0.2081 (10)	0.3239 (7)	0.4381 (6)	53 (2)
C(11)	−0.0777 (12)	0.3318 (9)	0.6209 (8)	88 (2)
C(12)	−0.0139 (11)	0.2598 (9)	0.5268 (7)	73 (3)
C(13)	0.1602 (10)	0.4600 (8)	0.1723 (6)	52 (2)
C(14)	0.2346 (10)	0.1017 (7)	0.3419 (6)	50 (2)

[a] Esd's in parentheses. [b] $U_{eq} = {}^1/_3\sum_i\sum_j U_{ij}a_i^*a_j^*a_ia_j \cos\alpha$.

Table IV. Atomic Coordinates and Isotropic Thermal Parameters (10^3 Å^2) for Polymorph B of $Fe(C_6H_8N_2S_2)_2(NCS)_2$[a]

atom	x	y	z	U_{eq}[b]
Fe	0.2501 (1)	0.0959 (1)	0.7501 (1)	145 (1)
S(1)	0.2833 (3)	−0.3151 (3)	0.4426 (2)	207 (1)
S(2)	−0.0852 (2)	−0.4502 (2)	0.3963 (2)	198 (1)
S(3)	0.2164 (2)	−0.0416 (3)	1.0572 (2)	200 (1)
S(4)	0.5856 (2)	0.2391 (3)	1.1037 (2)	190 (1)
S(5)	−0.1157 (3)	0.2222 (3)	0.7682 (3)	278 (2)
S(6)	0.6258 (3)	0.5700 (3)	0.7320 (3)	303 (2)
N(1)	0.3293 (6)	−0.0608 (7)	0.6501 (6)	152 (4)
N(2)	0.0520 (6)	−0.1343 (7)	0.5746 (5)	150 (4)
N(3)	0.1696 (6)	−0.0405 (7)	0.8499 (6)	153 (4)
N(4)	0.4476 (6)	0.2388 (7)	0.9256 (6)	155 (4)
N(5)	0.1143 (7)	0.1799 (8)	0.7958 (6)	200 (4)
N(6)	0.3852 (7)	0.2690 (9)	0.7035 (6)	208 (4)
C(1)	0.2294 (8)	−0.1984 (9)	0.5433 (7)	33 (2)
C(2)	0.4684 (10)	−0.1800 (10)	0.5683 (8)	56 (2)
C(3)	0.4824 (9)	−0.0254 (10)	0.6664 (8)	46 (2)
C(4)	0.0738 (8)	−0.2449 (9)	0.5114 (7)	34 (2)
C(5)	−0.2075 (11)	−0.3867 (12)	0.4445 (10)	67 (3)
C(6)	−0.1102 (9)	−0.1995 (10)	0.5315 (8)	48 (2)
C(7)	0.2699 (8)	0.0284 (9)	0.9556 (7)	32 (2)
C(8)	0.0308 (10)	−0.2181 (11)	0.9314 (8)	56 (2)
C(9)	0.0168 (9)	−0.1756 (10)	0.8321 (8)	45 (2)
C(10)	0.4266 (8)	0.1697 (9)	0.9889 (7)	29 (2)
C(11)	0.7087 (12)	0.3762 (13)	1.0559 (10)	72 (3)
C(12)	0.6096 (9)	0.3790 (10)	0.9685 (8)	49 (2)
C(13)	0.0185 (9)	0.1973 (9)	0.7839 (7)	39 (2)
C(14)	0.4816 (9)	0.3953 (10)	0.7161 (7)	35 (2)

[a] Esd's in parentheses. [b] $U_{eq} = {}^1/_3\sum_i\sum_j U_{ij}a_i^*a_j^*a_ia_j \cos\alpha$.

Details of this work will be the subject of a future publication.

B. Description of the Two Structures. Final atomic coordinates for non-hydrogen atoms are given in Tables III and IV, important distances and bond angles in Tables V and VI, and the ORTEP diagrams of the individual molecules in Figures 8 and 9. It is immediately apparent that the two modifications are similar with both having the cis configuration with very similar corresponding N–Fe–N angles. In general the Fe–N bonds are slightly shorter in modification A than in modification B but show a larger deviation from one another. Thus the average Fe–N bond to the thiazoline group in A is 2.20 Å and in B is 2.22 Å although the bond lengths range from 2.174 (6) to 2.242 (6) Å in A but only from 2.214 (6) to 2.232 (6) Å in B. This is better exemplified by the Fe–N bonds to the thiocyanate groups, which in B are identical at 2.082 (7) Å but which are 2.061 (7) and 2.079 (7) Å in A.

Table V. Important Interatomic Distances (Å) for Polymorphs A and B of $Fe(C_6H_8N_2S_2)_2(NCS)_2$[a]

	A	B		A	B
Fe–N(1)	2.197 (6)	2.225 (6)	S(1)–C(1)	1.718 (8)	1.730 (7)
Fe–N(2)	2.195 (6)	2.216 (6)	S(1)–C(2)	1.82 (1)	1.815 (9)
Fe–N(3)	2.242 (6)	2.232 (6)	S(2)–C(4)	1.724 (8)	1.748 (7)
Fe–N(4)	2.173 (6)	2.214 (6)	S(2)–C(5)	1.794 (9)	1.81 (1)
Fe–N(5)	2.079 (7)	2.082 (7)	S(3)–C(7)	1.739 (8)	2.078 (7)
Fe–N(6)	2.061 (7)	2.082 (7)	S(3)–C(8)	1.800 (9)	1.820 (9)
N(1)–C(1)	1.281 (9)	1.284 (9)	S(4)–C(10)	1.726 (8)	1.744 (7)
N(2)–C(4)	1.281 (9)	1.268 (9)	S(4)–C(11)	1.781 (1)	1.81 (1)
N(3)–C(7)	1.266 (9)	1.277 (9)	S(5)–C(13)	1.607 (9)	1.621 (8)
N(4)–C(10)	1.274 (9)	1.268 (9)	S(6)–C(14)	1.62 (1)	1.620 (8)
N(5)–C(13)	1.140 (9)	1.156 (9)	C(2)–C(3)	1.53 (1)	1.52 (1)
N(6)–C(14)	1.133 (9)	1.163 (3)	C(5)–C(6)	1.52 (1)	1.49 (1)
N(1)–C(3)	1.471 (10)	1.487 (9)	C(8)–C(9)	1.52 (1)	1.53 (1)
N(2)–C(6)	1.463 (9)	1.478 (9)	C(11)–C(12)	1.54 (1)	1.50 (1)
N(3)–C(9)	1.457 (10)	1.482 (9)	C(1)–C(4)	1.47 (1)	1.46 (1)
N(4)–C(12)	1.466 (10)	1.478 (9)	C(7)–C(10)	1.45 (1)	1.47 (1)
Fe---S(1)	4.638	4.662	N(1)---N(2)	2.644	2.672
Fe---S(2)	4.629	4.718	N(3)---N(4)	2.643	2.675
Fe---S(3)	4.650	4.667	S(1)---S(2)	3.358	3.400
Fe---S(4)	4.622	4.631	S(3)---S(4)	3.352	3.407

[a] Numbers in parentheses are estimated standard deviations in the least significant digit.

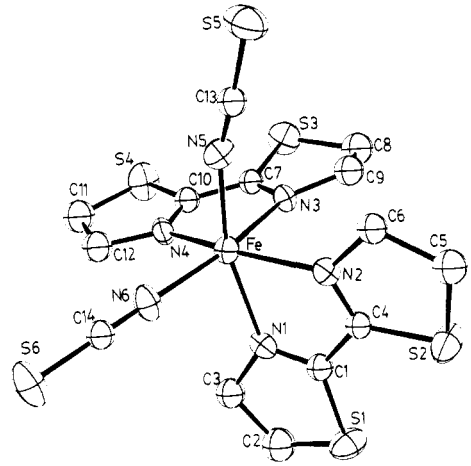

Figure 8. Molecular structure of polymorph A of $Fe(BT)_2(NCS)_2$.

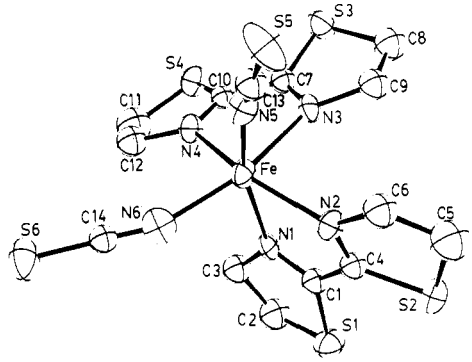

Figure 9. Molecular structure of polymorph B of $Fe(BT)_2(NCS)_2$.

The bond angles and bond lengths within each thiazoline group are essentially the same in both modifications as are the N–Fe–N bite angles at approximately 74°. The only slight difference in the two modifications is the general trend that the N–C and C–S bond lengths on average are slightly longer in B than in A. The tighter bonding within the thiazoline ring systems in A is demonstrated by shorter N---N and S---S distances in A than in B (see Table V). Similarly, the overall tighter bonding in A relative to that in B is indicated by the Fe---S distances within the thi-

Table VI. Bond Angles (deg) in the Polymorphs A and B of $Fe(C_6H_8N_2S_2)_2(NCS)_2$[a]

	A	B		A	B
N(1)–Fe–N(2)	74.0 (2)	74.0 (2)	N(2)–C(6)–C(5)	110.4 (6)	109.9 (7)
N(1)–Fe–N(3)	89.7 (2)	89.2 (2)	N(3)–C(7)–C(10)	118.9 (7)	117.8 (7)
N(1)–Fe–N(4)	95.1 (2)	88.6 (2)	N(3)–C(9)–C(8)	108.3 (7)	109.6 (7)
N(1)–Fe–N(6)	89.7 (2)	90.2 (2)	N(4)–C(10)–C(7)	117.2 (7)	118.1 (7)
N(2)–Fe–N(3)	88.3 (2)	88.4 (2)	N(4)–C(12)–C(11)	109.4 (8)	110.0 (7)
N(3)–Fe–N(4)	73.5 (2)	74.0 (2)	N(1)–C(1)–S(1)	120.0 (6)	119.7 (6)
N(4)–Fe–N(6)	91.2 (2)	88.9 (2)	N(2)–C(4)–S(2)	119.2 (6)	118.3 (6)
N(2)–Fe–N(6)	106.3 (2)	107.9 (2)	N(3)–C(7)–S(3)	118.3 (6)	119.6 (6)
N(2)–Fe–N(5)	88.3 (2)	88.4 (2)	N(4)–C(10)–S(4)	119.0 (6)	118.4 (5)
N(3)–Fe–N(5)	87.9 (2)	90.1 (2)	N(5)–C(13)–S(5)	177.2 (8)	179.6 (5)
N(4)–Fe–N(5)	101.1 (2)	108.1 (2)	N(6)–C(14)–S(6)	178.6 (8)	179.2 (7)
N(5)–Fe–N(6)	97.3 (3)	95.6 (3)	S(1)–C(1)–C(4)	123.1 (6)	123.4 (6)
N(1)–Fe–N(5)	162.2 (2)	162.4 (2)	S(1)–C(2)–C(3)	105.8 (6)	106.8 (6)
N(2)–Fe–N(4)	159.0 (2)	155.5 (2)	S(2)–C(4)–C(1)	123.2 (6)	122.6 (6)
N(3)–Fe–N(6)	164.6 (2)	162.9 (2)	S(2)–C(5)–C(6)	107.6 (6)	108.0 (7)
Fe–N(1)–C(1)	115.6 (5)	114.6 (5)	S(3)–C(7)–C(10)	122.8 (6)	122.6 (6)
Fe–N(1)–C(3)	131.9 (5)	132.9 (5)	S(3)–C(8)–C(9)	106.9 (6)	106.6 (6)
Fe–N(2)–C(4)	115.0 (5)	114.1 (5)	S(4)–C(10)–C(7)	123.8 (7)	123.4 (6)
Fe–N(2)–C(6)	131.8 (5)	131.8 (5)	S(4)–C(11)–C(12)	107.7 (7)	107.4 (7)
Fe–N(3)–C(7)	113.5 (5)	114.0 (5)	C(1)–S(1)–C(2)	89.7 (4)	89.3 (4)
Fe–N(3)–C(9)	132.0 (5)	132.9 (5)	C(4)–S(2)–C(5)	90.3 (4)	89.3 (4)
Fe–N(4)–C(10)	116.5 (5)	114.5 (5)	C(7)–S(3)–C(8)	88.8 (4)	89.2 (4)
Fe–N(4)–C(12)	130.2 (5)	131.4 (5)	C(10)–S(4)–C(11)	90.7 (4)	89.7 (4)
Fe–N(5)–C(13)	163.3 (7)	160.4 (6)	C(1)–N(1)–C(3)	111.3 (7)	111.1 (6)
Fe–N(6)–C(14)	178.1 (7)	159.8 (6)	C(4)–N(2)–C(6)	112.3 (6)	112.6 (6)
N(1)–C(1)–C(4)	116.8 (7)	116.8 (7)	C(7)–N(3)–C(9)	113.2 (7)	111.9 (6)
N(1)–C(3)–C(2)	110.0 (7)	109.8 (7)	C(10)–N(4)–C(12)	113.1 (7)	112.5 (6)
N(2)–C(4)–C(1)	117.6 (7)	119.0 (7)			

[a] Numbers in parentheses are estimated standard deviations in the last significant digit.

azoline groups, which average 4.635 Å in A and 4.669 Å in B.

The arrangements of the thiocyanate groups show significant differences in the two molecules. In modification B the two Fe–NCS bond lengths are identical, and the Fe–N–C and N–C–S angles are approximately 160 and 180°, respectively, in both Fe–N–C–S linkages. However, in modification A one of the Fe–N–C–S linkages is similar to the two in modification B but the other, Fe–N(6)–C(14)–S(6), has an essentially linear Fe–N–C angle of 178.1 (7)°.

Discussion

A. Polymorph A. The X-ray structure of the low-spin phase could not be done because our diffractometer does not have the necessary low-temperature accessories. The EPR results do tell us, however, that the low-temperature phase cannot be very much different from the high-temperature phase. The principal axes for the Mn^{2+} zero-field interaction are oriented exactly the same in both phases. This means that there was no change in the spatial orientation of the molecules in the lattice. Further, it can be seen in Figure 5 that the zero-field parameters of Mn^{2+} are, within experimental error, the same just above and below the transition temperature. This means there was no major change in the packing of the molecules in the lattice. In fact, as far as the EPR parameters are concerned, the only difference in the two phases is a difference in the thermal expansion effects in the zero-field interaction as shown again in Figure 5. This difference is most likely due to the fact[1,2,23-25] that the iron–ligand bonds are considerably shorter in the low-spin compounds than in the high-spin compounds. The smaller size of the low-spin molecules could therefore result in a larger thermal expansion coefficient for the low-temperature phase.

The effect of crystal dimensions on the rate of the high-spin to low-spin transition is interesting. To our knowledge, no one has investigated the "spin-crossover" transition of Fe(II) compounds in large single crystals of the type used in this study. There have been several studies of the effect of grinding upon the LS–HS transition in Fe(III) complexes[26-28] and in Fe(II) complexes,[5] but the original crystals were very much smaller than the crystals studied here. Grinding in these systems caused the fraction of high spin vs temperature curve to become more gradual and the temperature, T_c, at which there is 50% high spin to become lower. Further, after grinding there was always some portion of the iron atoms that remained in the high-spin state at all temperatures. These effects were attributed not to smaller size of the crystallites but to the increased number of defect sites created by the grinding. We have found the same transition temperatures and the same range of hysteresis for single crystals, powders precipitated normally from solution, and powders created by grinding large single crystals for the system studied here. The only difference between the powder and the large crystals was the rate of change for the high-spin to low-spin transition. The rate of the reverse transition (low spin to high spin) was fast in all cases due to the rapid pulverization of the single crystals when the transition started.

There are very few reports of measurements on the rate of the "spin-crossover" transition. Müller et al.[5] mentioned a slow HS–LS transition rate in the "extracted" sample of polymorph A. The transition in $[Fe^{II}(o\text{-phen})_2(SCN)_2]$ powders has been reported as taking 15 min[8] to hours[29] depending on the method of preparation.

The line widths in the paramagnetic phase increased continuously with cooling from room temperature down to 77 K, but the increase was much less dramatic than that observed in polymorph B crystals. The line widths of the low-spin resonance were not significantly temperature dependent, but the $(-^1/_2 \leftrightarrow {}^1/_2)$ transitions in the low-spin resonance had much smaller line widths than those found in the paramagnetic resonance. Moreover, the line widths observed for the diamagnetic component during the slow HS–LS transition at 77 K were independent of the actual concentration of the paramagnetic species. This means that most of the Mn ions in the diamagnetic phase were not near any

(23) Greenaway, A. M.; O'Connor, C. J.; Schrock, A.; Sinn, E. *Inorg. Chem.* **1979**, *18*, 2692.
(24) Mikami, M.; Konno, M.; Saito, Y. *Acta Crystallogr., Sect. B: Struct. Crystallogr. Cryst. Chem.* **1980**, *B36*, 275.
(25) Wiehl, L.; Kiel, G.; Kohler, C. P.; Spiering, H.; Gütlich, P. *Inorg. Chem.* **1986**, *25*, 1565.
(26) Federer, W. D.; Hendrickson, D. N. *Inorg. Chem.* **1984**, *23*, 3870.
(27) Haddad, M. S.; Lynch, M. W.; Federer, W. D.; Hendrickson, D. N. *Inorg. Chem.* **1981**, *20*, 131.
(28) Haddad, M. S.; Federer, W. D.; Lynch, M. W.; Hendrickson, D. N. *J. Am. Chem. Soc.* **1980**, *102*, 1468.
(29) Casey, A. T.; Isaac, F. *Aust. J. Chem.* **1967**, *20*, 2765.

paramagnetic iron atoms even when most of the iron atoms in the crystal were still paramagnetic. It has been suggested[6] that the spin transition in this compound involves domains or clusters containing an average of 50–55 molecules. Our results on single crystals indicate that the domains are much larger in these crystals because a domain of only 50–55 molecules, randomly dispersed throughout the crystal, would have better than 80% of the molecules on the surface of the domain and therefore most of the Mn ions would be adjacent to one or more paramagnetic iron atoms.

One could argue that the impurity Mn complexes catalyze the conversion from high spin to low spin and are therefore always found in the center of the domain, but this seems highly unlikely since the presence of the Mn complexes has no effect on the transition or its hysteresis.

The dependence of the rate of transition on crystal size could be connected to the problem of domain size discussed above. It may be unique to this system or quite common. We do know that it does not appear[30] when the EPR spectrum of Mn^{2+} is examined in a single crystal of $[Fe^{II}(2\text{-}(NH_2CH_3)py)_3]Cl_2\cdot EtOH$, which has a gradual spin transition over an extended temperature interval. Our results suggest that the transition from high to low spin starts at very few sites and there are less such sites in the larger crystals. Further, these domains grow into larger domains by spin changes at the domain boundaries. For example, the preferred origin of the spin change could be on crystal faces. This would explain the slower rate in large crystals and the lack of line width changes in the low-spin spectrum as the spin change takes place. This does not exclude the spin conversion taking place in units of 50–55 molecules, it just requires that any crossover in spin occur next to a region that is already low spin. The fracturing of the crystal when the transition goes from low to high spin is not surprising since it involves an expansion of the lattice. Expansion of a few sites will cause internal pressures to develop that will rapidly fracture the crystal along various fracture planes. The transition can go faster by fracturing since the growth of domains is too slow.

B. Polymorph B. The results of the X-ray investigations do not confirm the presumption of the pseudoaxial molecular symmetry suggested by the small E/D ratio, but the two bithiazoline ligands and the two thiocyanate anions appear to be equivalent. The geometrical relation of the bithiazoline containing N(1) and N(2) to the thiocyanate with N(5) is similar to the relation of the second bithiazoline to the thiocyanate with N(6): the angle N(3)–Fe–N(6) is equal to the angle N(1)–Fe–N(5) and the angle N(2)–Fe–N(6) is equal to N(4)–Fe–N(5). The iron atom deviates from both planes N(4)N(2)N(5) and N(3)N(4)N(6) by less than 0.005 Å, while the corresponding deviations are of some 0.04 Å in polymorph A. Thus, there are two equivalent groups of ligands and the molecule is more ordered than that of polymorph A. This may be the reason for the considerable difference in the E parameters for both crystalline forms. It should be noted, however, that the Mn ion does not necessarily assume the exact geometry of the iron ions. The E parameter is extremely sensitive to the changes in the environment of the manganese atoms. The increase of the zero-field splitting with decreasing temperature is caused by a decrease in the lattice constants. The much stronger temperature dependence of the line width in polymorph B relative to that of the paramagnetic phase in polymorph A indicates a weaker coupling of the electronic and phonon systems in this crystal.

C. Crystal Structure and the "Crossover" Phenomenon. The preparation of two crystalline forms with drastically different thermomagnetic properties has given us a very rare, if not unique, opportunity to look for the interactions responsible for the "crossover" phenomenon. There are some small but significant differences between both molecular structures. All the Fe–N bonds (except Fe–N3) in polymorph A are slightly shorter than those in polymorph B, resulting in the average Fe–N distances of 2.158 and 2.175 Å for the A and B forms, respectively. It is interesting to compare the iron–thiocyanate nitrogen bond lengths in both forms. In the A form the thiocyanate with a Fe–N–C angle of 163° shows an Fe–N distance of 2.079 Å, very similar to both Fe–N(thiocyanate) distances in the B form, where both Fe–N–C angles are about 160°. The second thiocyanate anion in the A form is bound almost coaxially with the corresponding Fe–N bond—the Fe–N–C angle is equal to 178° and the Fe–N distance is much shorter—2.061 Å. There is an apparent trend to shortening the Fe–N bonds with increasing Fe–N–C angle, thus indicating the importance of π-bonding in this system. The shorter iron–ligand bonds in the A form probably cause the ligand field to be somewhat stronger than in the B modification, thus bringing the molecule nearer to the "crossover" point.

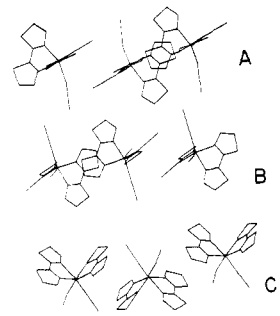

Figure 10. Arrangement of three molecules showing the chain of the interactions between the thiazoline rings in polymorph A: (A) view with N(2)–C(4)–S(2)–C(5)–C(6) rings in the plane of the paper; (B) view with N(4)–C(10)–S(4)–C(11)–C(12) rings in the plane of the paper; (C) view along a direction forming angles of 115, 46, and 69° with Fe–N(1), Fe–N(2), and Fe–N(3), respectively.

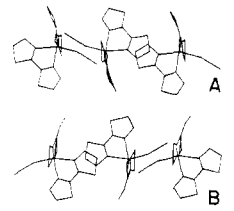

Figure 11. Chain of interactions between the thiazoline rings in polymorph B: (A) the least-squares plane N(1)–C(3)–C(2)–S(1)–C(1) in the plane of the paper; (B) the least-squares plane N(3)–C(9)–C(8)–S(3)–C(7) in the plane of the paper.

It has been suggested before[1,2,4-9] that the "crossover" phenomena in the solid complexes are of a cooperative nature. This has also been confirmed by the results obtained in this work. The growth of a new domain during the phase transition requires the propagation of information about the change of the spin state of a given iron ion to other iron ions. This information is transmitted through the strains or internal pressures caused by the differences in the dimensions of the high- and low-spin molecules. Thus, we should also consider the crystal packing of both A and B modifications to look for differences in intermolecular interactions that might account for the "crossover" in the A form. One molecule was picked out as the basic one, and the shortest intermolecular distances between it and 26 similar molecules as well as 27 enantiomeric molecules in the neighboring unit cells were determined. Chains of close contacts between the thiazoline rings are found in both forms.

In the A modification the approximately planar ring N(2)–C(4)–S(2)–C(5)–C(6) (largest dihedral angle 4.44°) lies on top of the same ring in the adjacent molecule with a 3.8-Å separation between the planes. The nearly planar ring systems N(4)–C(10)–S(4)–C(11)–C(12) (largest dihedral angle 3.18°) are again positioned on top of one another (see Figure 10) and separated by 4.0 Å. (The corresponding rings in all molecules are parallel to each other because they are joined via the inversion center and/or translations.)

In the B form the ring systems N(1)–C(1)–C(2)–S(1)–C(3) deviate much more from planarity (the largest dihedral angle is 15.4°) and are not positioned as exactly on top of each other as they are in the A modification. The arrangement of the rings N(3)–C(7)–C(8)–S(3)–C(9) is nearly equivalent to the ar-

(30) Doan, P. E.; McGarvey, B. R., private communication.

rangement of the rings N(1)-C(1)-C(2)-S(1)-C(3) (see Figure 11).

It seems that these interactions may be more effective in the A form. Moreover, the chains of close contacts between the sulfur atoms are apparent. The corresponding intermolecular distances are S(1)-S(5) = 3.35 Å for A and S(2)-S(4) = 3.61 Å, S(1)-S(6) = 3.42 Å, and S(3)-S(5) = 3.42 Å for the B form. It would appear that the structure of polymorph A allows for more effective intermolecular interactions (despite the lower density) than the structure of polymorph B does. The difference between both structures is not very dramatic, however.

Conclusions

This is, to our knowledge, the first case of two polymorphs of an iron(II) compound in which the "spin-crossover" behavior is seen in only one modification. The complex bis(thiocyanato)-bis(2,2'-bipyridyl)iron(II) forms three polymorphs. All three exhibit the "spin crossover" at similar temperatures, however.[31] The triclinic modification of bis(3-chloropyridine)(octaethylporphinato)iron(III) perchlorate exhibited a $S = {}^1/_2 \leftrightarrow S = {}^5/_2$ spin transition,[32,33] while the monoclinic form had the iron in a mixed ${}^3/_2$-${}^5/_2$ spin state. In this case there were distinct differences in the orientation of the 3-Cl-py ligand that readily explained the difference in behavior. In the system studied here, the two structures are very similar and it was difficult to pin down any differences that could be called key factors.

The EPR parameters observed for the low- and high-spin phases indicate that the change in crystal geometry must be very minor during the phase transition. EPR line widths of the low-spin resonance observed during the spin transition in large crystals have shown that the transition involves rather larger domains than have been proposed in studies on powders. The dependence of the rate of the high- to low-spin transition on crystal size suggests that the domains start at a few centers and that there are fewer such centers in the larger single crystals.

Acknowledgment. This work was supported by the Natural Sciences and Engineering Research Council of Canada.

Registry No. BT, 41601-87-0; $Fe(BT)_2(NCS)_2$, 60105-57-9; $Mn(BT)_2(NCS)_2$, 112219-55-3; dithiooxamide, 79-40-3; 2-aminoethanol, 141-43-5; *N,N'*-bis(2-hydroxyethyl)dithiooxamide, 120-86-5; thionyl chloride, 7719-09-7; 2,2'-bi-2-thiazoline dihydrochloride, 41601-88-1.

Supplementary Material Available: Tables SI-SIV, listing the anisotropic thermal parameters for non-hydrogen atoms, hydrogen atom coordinates, and isotropic thermal parameters (4 pages); tables of calculated and observed structure factors (20 pages). Ordering information is given on any current masthead page.

(31) König, E.; Madeja, K.; Watson, K. J. *J. Am. Chem. Soc.* **1968**, *90*, 1146.
(32) Scheidt, W. R.; Geiger, D. K.; Haller, K. J. *J. Am. Chem. Soc.* **1982**, *104*, 495.
(33) Scheidt, W. R.; Geiger, D. K.; Hayes, R. G.; Lang, G. *J. Am. Chem. Soc.* **1983**, *105*, 2625.

Contribution from the Chemistry Division and Laboratory for the Structure of Matter, U.S. Naval Research Laboratory, Washington, D.C. 20375-5000

Transition-Metal-Promoted Oxidation of Organic Sulfides. Synthesis, Characterization, and Structure of (μ_4-Oxo)hexakis(μ_2-chloro)tetrakis(dialkyl sulfoxide)tetracopper(II)

Joseph T. Guy, Jr.,[†] John C. Cooper,*[†] Richard D. Gilardi,[‡] Judith L. Flippen-Anderson,[‡] and Clifford F. George, Jr.[‡]

Received August 10, 1987

The transition-metal-promoted dioxygen oxidation of thioethers was examined under ambient reaction conditions. Direct reactions of $CuCl_2 \cdot 2H_2O$ with alkyl thioethers is shown to yield the unique copper tetramer $Cu_4Cl_6O(OSR_2)_4$ (R = ethyl (**1**), *n*-butyl (**2**)) upon oxidation. These complexes were examined by IR, UV-vis, and X-ray diffraction techniques. The species $Cu_4Cl_6O(OS(CH_2CH_3)_2)_4$ was determined by X-ray crystallography to contain a central μ_4-oxide surrounded pseudotetrahedrally by four trigonal-bipyramidal Cu(II) atoms. The five-coordinate copper atoms have bridging chlorides in the equatorial position with the μ_4-oxygen and a sulfoxide oxygen in the axial positions. The complex crystallizes in the orthorhombic noncentrosymmetric space group $P2_12_12_1$ with a = 10.436 (2) Å, b = 11.092 (2) Å, and c = 29.679 (7) Å. Final discrepancy values of R = 0.049 (R_w = 0.059) were obtained from 2378 unique, observed reflections. Distortions from ideal symmetry are observed in the $\{Cu_4O\}$ core, in which the Cu-O_{cen} bond distances range from 1.883 (7) to 1.911 (7) Å. The equatorial planes of the five-coordinate coppers are also distorted from true trigonal-bipyramidal geometry with Cu-Cl bond distances ranging from 2.360 (3) to 2.451 (3) Å and Cl-Cu-Cl bond angles ranging from 109.4 (1) to 129.4 (1)°. The IR spectra of the complexes show $\nu_{S=O}$ stretches of 956 and 930 cm^{-1} and ν_{Cu-O} of 585 and 583 cm^{-1} for **1** and **2**, respectively. The formation mechanism is proposed to involve a Cu^I-SR^2 intermediate followed by air oxidation to the Cu^{II} tetramer with coordinated sulfoxide ligands.

Introduction

The chemistry of Cu^{II} with sulfur donor ligands has important implications in a variety of diverse areas. These include the naturally occurring blue copper proteins[1] and the copper-promoted oxidation of thioethers to sulfoxides.[2] Copper complexes of chelating, multidentate ligands with cyclic thioethers have been studied extensively in the past due to the enhanced stability of the Cu-S bond in such complexes.[3] In contrast, relatively little is known about Cu^{II} reactions with less complex thioethers. Simple alkyl thioethers tend to form more ephemeral copper compounds due to their weak coordination to the metal center and can readily reduce the Cu^{II} to Cu^{I}.[4] In light of this, we have undertaken a study of the reactivity of Cu^{II} with simple thioethers and have successfully characterized the reaction product of $CuCl_2$ with the alkyl thioethers $(C_2H_5)_2S$, $(CH_3(CH_2)_3)_2S$, and $((CH_3)_3C)_2S$ by IR and UV-visible spectra, elemental analysis, and X-ray dif-

*To whom correspondence should be addressed.
[†]Chemistry Division.
[‡]Laboratory for the Structure of Matter.

(1) Colman, P. M.; Freeman, H. C.; Guss, J. M.; Murata, M.; Norris, V. A.; Ramshaw, J. A. M.; Venkatappa, M. P. *Nature (London)* **1978**, *272*, 319.
(2) Ainscough, E. W.; Brodie, A. M.; Husbands, J. M.; Gainsford, G. J.; Gabe, E. J.; Curtis, N. F. *J. Chem. Soc., Dalton Trans.* **1985**, 151.
(3) Hay, R. W.; Govan, N.; Pujari, M. P. *J. Chem. Soc., Dalton Trans.* **1987**, 963. Micheloni, M.; Paoletti, P.; Siegfried-Hertli, L.; Kaden, T. A. *J. Chem. Soc., Dalton Trans.* **1985**, 1169. Sigel, H.; Rheinberger, V. M.; Fischer, B. E. *Inorg. Chem.* **1979**, *18*, 3334.
(4) Baek, H. K.; Karlin, K. D.; Holwerda, R. A. *Inorg. Chem.* **1986**, *25*, 2347. Baek, H. K.; Holwerda, R. A. *Inorg. Chem.* **1983**, *22*, 3452.

This article not subject to U.S. Copyright. Published 1988 by the American Chemical Society